Galvanic Coupling Between Pure Copper and Pure Aluminum

Experimental Approach and Mathematical Model

Jean-Baptiste Jorcin,[a] Christine Blanc,[a,*] Nadine Pébère,[a,*,z] Bernard Tribollet,[b,*] and Vincent Vivier[b,*]

[a]*Centre Interuniversitaire de Recherche et d'Ingénierie des Matériaux, UMR CNRS 5085-ENSIACET, 31077 Toulouse Cedex 04, France*
[b]*Laboratoire Interfaces et Systèmes Electrochimiques, UPR 15 du CNRS, Université Pierre et Marie Curie, 75252 Paris Cedex 05, France*

The corrosion behavior of a pure aluminum/pure copper couple in a weakly conductive sulfate solution was investigated. Potential and current distributions on the surface of the model couple at the beginning of immersion were obtained by solving the Laplace equation using a finite element method (FEM) algorithm. The potential distribution predicted by the calculations was checked using a Ag/AgCl microreference electrode. A good agreement was found between experimental and theoretical results. It was shown that the reaction occurring at the copper electrode was oxygen reduction, while aluminum remote from the Al/Cu interface remained in the passive state. Moreover, calculations predicted a large cathodic current, related to an increase in oxygen reduction, restricted to copper at the Al/Cu interface. This led to a local pH increase reaching values higher than 9, allowing the dissolution of aluminum to occur close to the interface. Combining these data with optical and scanning electron microscope observations after 24 h of immersion in the sodium sulfate solution allowed a three-step mechanism to be proposed to explain the corrosion damage, and particularly the presence of a copper deposit on the aluminum surface, some distance from the Al/Cu interface, a phenomenon currently observed in commercial copper-rich aluminum alloys.

DOI: 10.1149/1.2803506

There is significant interest in the corrosion behavior of Cu-containing Al alloys, such as the 2024 aluminum alloy (AA2024), which remain of importance for aerospace applications due to their high strength-to-weight ratio. Consequently, the corrosion susceptibility of 2XXX Al-alloy series has been studied for a long time.[1-12] The corrosion of AA2024 is mainly caused by the heterogeneous microstructure of the alloy, which has been intentionally developed to improve the mechanical properties of the material.

Among the different types of intermetallic particles present in AA2024 alloy, both coarse Al_2CuMg particles, also called S-phase or Al–Cu–Mn–Fe particles (size: 1–30 μm) and smaller Al_2CuMg particles (about 200 nm) present in the grain boundaries have been widely studied due to their reactivity that constitutes initiation sites for corrosion.[13-20] Even though the influence of copper-rich intermetallics on the corrosion resistance of aluminum alloys was clearly shown, the mechanisms explaining the dissolution of the intermetallics, the copper enrichment, and the pit nucleation at these sites are still not clearly explained.[13-23] Authors usually refer to a galvanic coupling phenomenon between the particles and the surrounding matrix. Zhu and Van Ooij[24] showed that anodic Al_2CuMg particles dealloyed both Al and Mg (with a more severe dealloying of the Mg) when immersed in a neutral 0.6 M sodium chloride solution. Simultaneously, a significant dissolution of the Al matrix surrounding the coarse particles was also observed. This mechanism is similar to that proposed by other authors.[15,18,25] In previous studies, Blanc et al.[13,14] discussed a slightly different mechanism, in which the copper-rich intermetallic reactivity was studied in a 0.1 M sulfate solution and described by a three-step process consisting of homogeneous dissolution of the particle, copper redeposition, followed by local dissolution of the matrix surrounding the particle. These phenomena have been widely investigated by electrochemical measurements in combination with scanning electron microscopy (SEM) and electron dispersive spectroscopy (EDS). However, conventional electrochemical methods lack spatial resolution, while microscopy techniques do not allow the in situ chemical composition to be determined; these are crucial for the understanding of the role of the intermetallic particles on the corrosion process. Consequently, many authors have used atomic force microscopy (AFM), which provides high lateral resolution to study dissolution phenomena occurring in the S-phase.[18,25-27]

To understand the corrosion behavior of copper-rich aluminum alloys, another alternative is to study the electrochemical behavior of model alloys that are representative of the different metallurgical phases.[22,28] For example, thin films of Al–Cu alloys can be easily obtained using magnetron sputtering and are useful for such studies.[29,30] However, these alloys are mostly multiphase alloys and thus their corrosion behavior remains intricate.

In the present study, a simple system was considered consisting of a pure aluminum/pure copper (Al/Cu) couple. Sample immersion for 24 h in a 10^{-3} M Na_2SO_4 solution was followed by observations with an optical and a scanning electron microscope to reveal the corrosion morphology. Particular attention was paid to the Al/Cu interface. Measurements of local potentials were carried out and compared with results obtained from calculations based on the resolution of the Laplace equation to describe the first moments of immersion. On the basis of the experimental approach and the mathematical model, the interpretation of the corrosion phenomena occurring at the Al/Cu interface is proposed.

Experimental

Samples.— The sample consisted of a pure aluminum/pure copper couple. A cylinder of pure aluminum (99.999 wt %), provided by Alfa/Aesar, was drilled in its center and a cylinder of pure copper (99.9 wt %), provided by Goodfellow, was then introduced by force into the hole. The assembly of the two materials gave a perfectly joined interface, avoiding any crevice corrosion due to surface defects. The diameters of the two cylinders were chosen to obtain a ratio aluminum surface area/copper surface area of 10 (external diameters were equal to 10 and 3.15 mm for aluminum and copper bars, respectively). The electrode was then embedded in an epoxy resin so that a disk electrode was obtained at the extremity.

Before immersion in the electrolyte, the disk electrode was mechanically polished with SiC papers up to 4000 grade and ultrasonically cleaned with ethanol, then with distilled water. The electrolyte was a 10^{-3} M Na_2SO_4 solution prepared with analytical grade chemicals in contact with an air atmosphere and at room temperature.

Local electrochemical measurements.— Local electrochemical measurements were performed using a homemade device. The local

* Electrochemical Society Active Member.
z E-mail: Nadine.Pebere@ensiacet.fr

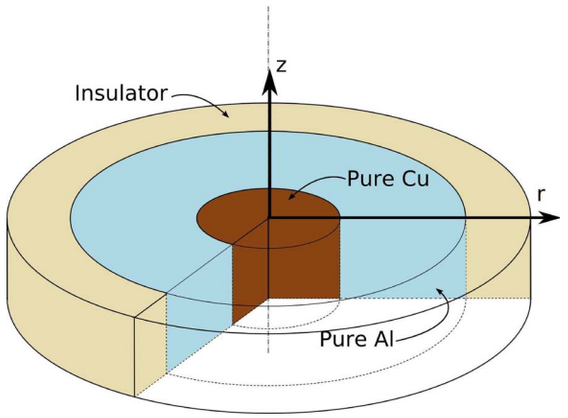

Figure 1. (Color online) Schematic representation of the pure aluminum/pure copper model couple.

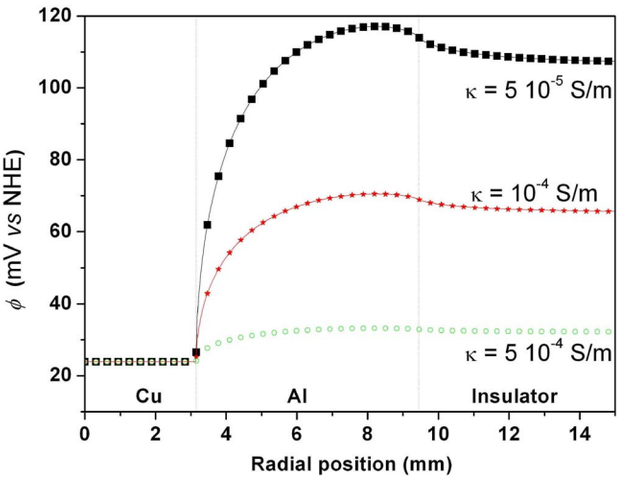

Figure 2. (Color online) Potential distributions on the surface of the Al/Cu model couple deduced from theoretical calculations for different values of electrolyte conductivity.

potential variations were measured using a 100 μm diameter Ag/AgCl microelectrode. It consisted of a Ag wire (100 μm in diameter, Goodfellow) laterally insulated with cataphoretic paint and sealed in a glass capillary with epoxy resin. The AgCl was deposited in a 2 M KCl solution under potentiostatic oxidation of the Ag electrode at 0.4 V/SCE. The microreference electrode was moved with a three-axis positioning system (UTM25, Newport) driven by a motion encoder (MM4005, Newport) allowing a spatial resolution of 0.2 μm in the three directions. A homemade analog differential amplifier with both variable gain and high input impedance was used to record the local potential. All measurements were performed at the corrosion potential E_{corr} using a Keithley 2000 digital multimeter. The experimental setup was controlled with homemade data-acquisition software developed under a LabView environment.

Surface characterizations.— The samples were observed before and after 24 h of immersion in a 10^{-3} M Na_2SO_4 solution by optical microscopy with an Olympus PMG3 microscope. Observations with a scanning electron microscope were also performed using a Leo 435VP apparatus to obtain a better description of the corrosion morphology, particularly at the Al/Cu interface.

Theoretical Description of the Current and Potential Distributions

Mathematical model.— Numerical simulations were performed to obtain a description of the potential and current distributions on the surface of the disk electrode and in the surrounding electrolyte solution at the beginning of immersion. Figure 1 gives a schematic representation of the disk electrode used in this study.

The potential Φ in the solution surrounding the electrode is governed by the Laplace equation

$$\nabla^2\Phi = 0 \qquad [1]$$

Using cylindrical coordinates (r,θ,z), Eq. 1 can be expressed as

$$\frac{1}{r}\frac{\partial}{\partial r}\left(r\frac{\partial\Phi}{\partial r}\right) + \frac{1}{r^2}\frac{\partial^2\Phi}{\partial\theta^2} + \frac{\partial^2\Phi}{\partial z^2} = 0 \qquad [2]$$

where z is the normal distance to the electrode surface, r is the radial coordinate, and θ is the azimuth. The cylindrical symmetry condition requires the geometry to be invariant under rotation about the y axis, i.e.,

$$\frac{\partial\Phi}{\partial\theta} = 0 \qquad [3]$$

The combination of Eq. 2 and 3 yields the governing equation in a two-dimensional (2D) domain as

$$\frac{\partial^2\Phi}{\partial r^2} + \frac{1}{r}\frac{\partial\Phi}{\partial r} + \frac{\partial^2\Phi}{\partial z^2} = 0 \qquad [4]$$

On the surrounding insulator and far from the electrode surface, the boundary conditions are given by

$$\left.\frac{\partial\Phi}{\partial z}\right|_{z=0} = 0 \quad \text{at } r > r_0 \qquad [5]$$

and

$$\Phi \to 0 \quad \text{as } r^2 + z^2 \to \infty \qquad [6]$$

Under the assumption of a kinetic regime, the current density at the electrode surface can be expressed as

$$\mathrm{I} = -\kappa \left.\frac{\partial\Phi}{\partial z}\right|_{z=0} \qquad [7]$$

where κ is the electrolyte conductivity.

The boundary conditions were determined from experimental measurements performed individually on each material. On the aluminum part of the electrode, the boundary condition corresponds to an anodic current of 1 μA cm^{-2}. On the copper electrode, both oxygen reaction and copper dissolution were taken into account. The global current can be expressed as

$$I_{Cu} = k_{Cu}\exp\left(\frac{2.303}{b_{Cu}} \times \Phi\right) - k_{O_2}\exp\left(-\frac{2.303}{b_{O_2}} \times \Phi\right) \qquad [8]$$

where the constants k_{Cu} and k_{O_2} are determined from experimental measurements of both the corrosion potential of the Cu electrode and the anodic and cathodic Tafel slopes of copper dissolution and oxygen reduction (b_{Cu}, b_{O_2}), respectively. The values determined experimentally were: E_{corr} = −0.610 V/SSE, b_{Cu} = 55 mV/dec, and b_{O_2} = 220 mV/dec, allowing calculation of the constants k_{Cu} = 9.4 A cm^{-2}, and k_{O_2} = 7.6 10^{-6} A cm^{-2}.

The simulations were performed using a finite element package Femlab in a 2D axial symmetry. The mesh size was refined to obtain a numerical error lower than 0.1% evaluated from the net current of the system, which is the sum of the current passing through the copper and aluminum electrodes.

Results of the simulations.— Figure 2 shows the potential distribution calculated on the electrode surface along the electrode radius with the electrolyte conductivity as a parameter. Independently of the electrolyte conductivity, the general shape of the potential distribution remains similar. The potential is seen to be constant over

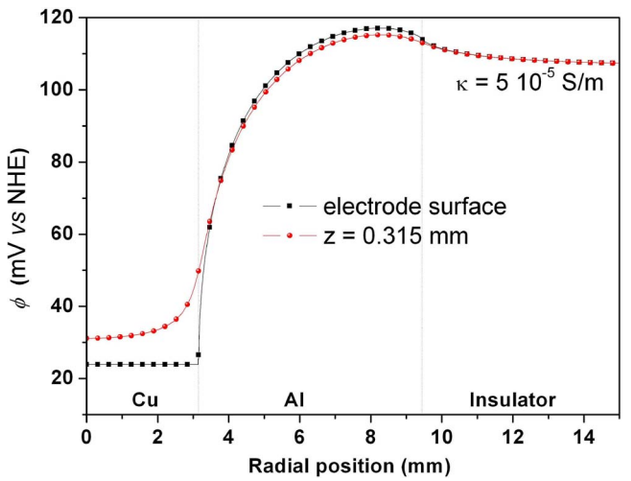

Figure 3. (Color online) Potential distributions on the surface of the Al/Cu model couple deduced from theoretical calculations for two values of the probe position (electrolyte conductivity equal to 5×10^{-5} S m^{-1}).

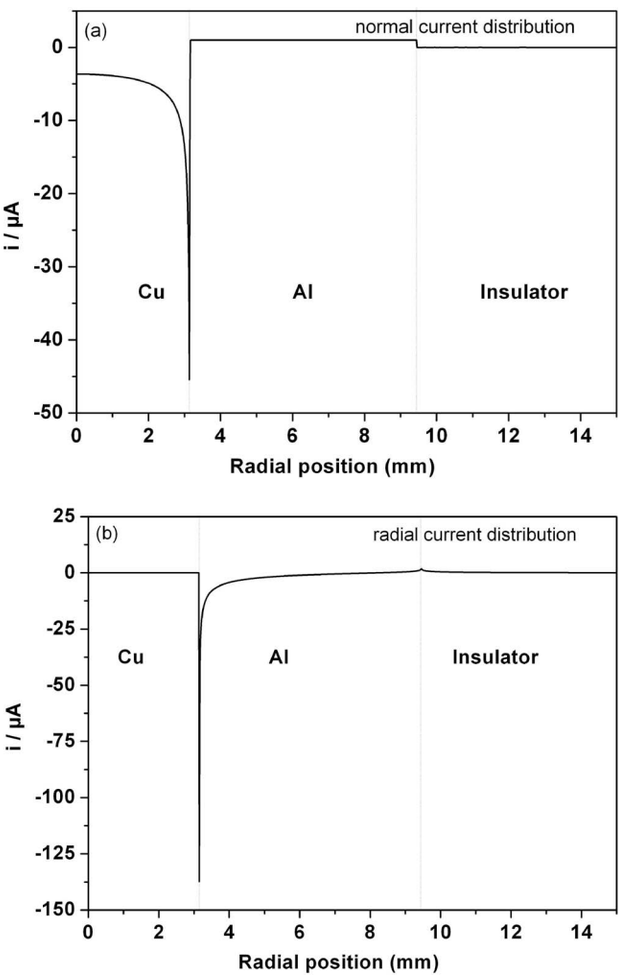

Figure 4. Current distributions on the surface of the Al/Cu model couple deduced from theoretical calculations: (a) normal current and (b) radial current.

the copper electrode; it strongly increases immediately after the Cu/Al interface and reaches a maximum value over the aluminum electrode near the Al/insulator interface just before a slight decrease. Such behavior is fully consistent with the boundary conditions determined for the calculation. Figure 2 also shows that the variations of the potential along the disk-electrode radius are higher for a low conductivity of the electrolyte which, from a practical point of view, made these variations easier to detect. Figure 3 shows the influence of Ag/AgCl probe position (i.e., readings at two distances from the electrode surface). Calculations were performed in the case of a weakly conductive electrolyte to highlight the influence of the position of the probe on the potential distribution. No significant difference was observed between the two measurements; when the probe was withdrawn from the electrode surface, the sudden variation of the potential at the Al/Cu interface was barely reduced by comparison to measurements performed on the disk electrode surface itself. Moreover, the amplitude of the potential variations was smaller when the electrode was far from the substrate.

The resolution of the Laplace equation also allows the distribution of the current on the disk electrode surface to be determined: both normal and radial current distributions were calculated as shown in Fig. 4. The normal current (Fig. 4a) on aluminum is constant and corresponds to the boundary condition chosen, while for the copper electrode, the calculations show a cathodic current distributed along the electrode radius. Thus, calculation led to results in good agreement with the initial hypothesis, a passive behavior for aluminum and a cathodic current related to oxygen reduction on copper. Furthermore, potential and current distributions revealed a particular behavior at the Al/Cu interface. Figure 4a shows a high cathodic current on copper at the Al/Cu interface corresponding to an increase of oxygen reduction on copper

$$O_2 + 2H_2O + 4e^- \rightarrow 4\ OH^- \qquad [9]$$

This suggests that local variations of the chemical composition of the electrolyte can occur from the beginning of immersion with a local alkalinization of the electrolyte at the Al/Cu interface. Figure 4b also shows an increase of the radial component of the current over the aluminum in the vicinity of the interface between the two metals. The variations of the radial contribution are linked to the potential distribution over the aluminum, whereas for a constant value of the potential at the electrode surface (for instance over the copper electrode as shown in Fig. 3) the normal contribution of the current varies from the electrode center to the Cu interface (Fig. 4a) and the radial current contribution is zero. These results suggested a particular evolution of the interface morphology of the disk electrode after immersion in the electrolyte related to corrosion phenomena restricted to the Al/Cu interface.

Results and Discussion

Morphology of the Al/Cu interface after 24 h of immersion in a 10^{-3} M Na_2SO_4 solution.— The Al/Cu interface was observed using optical microscopy and SEM before and after immersion in the sodium sulfate solution. Figure 5 shows an optical micrograph of the interface before immersion (copper on the right and aluminum on the left of the micrograph). The two materials are perfectly joined without any defects observable at the interface. After 24 h of immersion in the sulfate solution (Fig. 6a), two main differences were observed in the vicinity of the interface by comparison with the observations performed before immersion.

1. A deep crevice was formed at the Al/Cu interface. Close to the crevice, aluminum presents a bright color, while, except in this zone, it seems to be covered by an oxide film over its whole surface, which is in good agreement with previous hypotheses concerning a passive state for aluminum in the couple. The bright color suggests that the crevice was at least partially related to the dissolution of the aluminum close to the interface.

2. An orange-brown ring of about 50 μm thick occurred all around the Al/Cu interface. It was located on the aluminum material at a distance of about 150 μm from the interface. The ring was

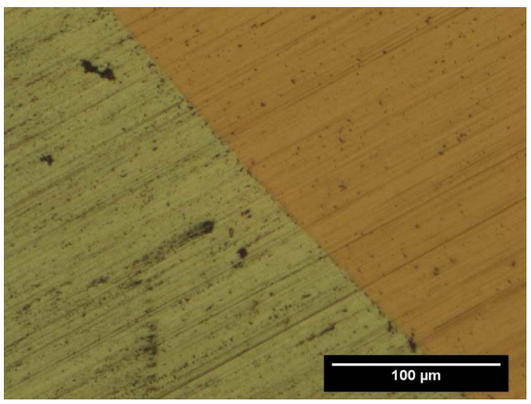

Figure 5. (Color online) Optical observation of the Al/Cu interface of the disk electrode before immersion.

analyzed by EDS as being copper and is attributed to the redeposition of copper coming from the dissolution of the Al/Cu interface.[31,32]

The observations also show that the corrosion processes were restricted to the Al/Cu interface and only concerned the interface or the zone close to the interface (copper ring at 150 µm from the interface). No other domain of the sample exhibited corrosion damage, whether on aluminum or copper. Moreover, Fig. 6b clearly

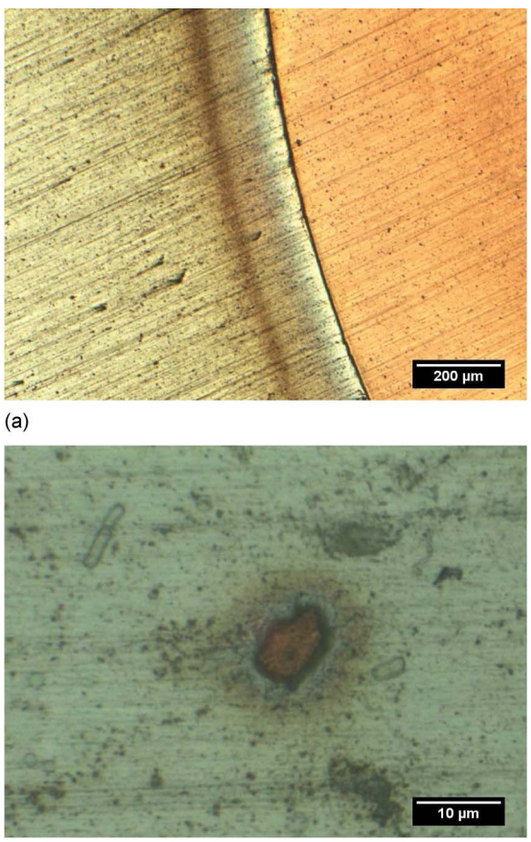

Figure 6. (Color online) Optical observations after 24 h of immersion in a 10^{-3} M Na_2SO_4 solution of (a) the Al/Cu interface and (b) a copper particle embedded in pure aluminum on the disk electrode.

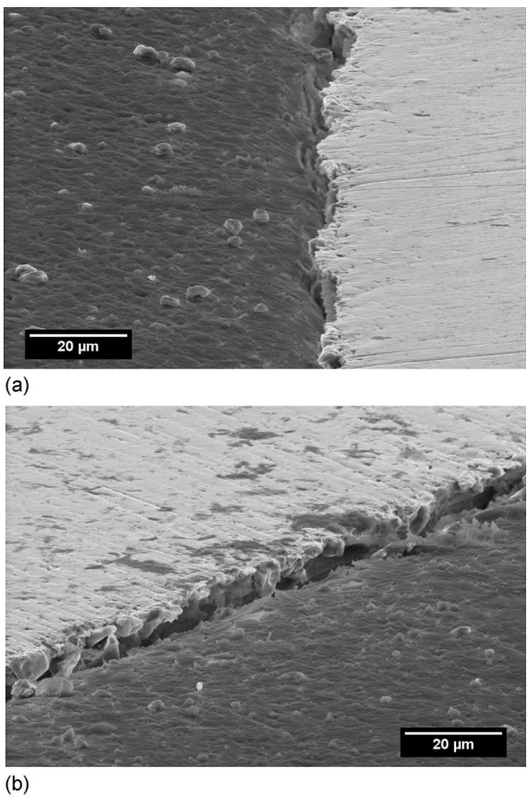

Figure 7. SEM observations of the Al/Cu interface of the disk electrode after 24 h of immersion in a 10^{-3} M Na_2SO_4 solution: (a) and (b) show two different views of the crevice.

shows that the corrosion phenomenon is independent of the size of the interface involved in the reaction process. Similar phenomena were observed around a 10 µm particle of copper which became embedded in the aluminum part of the electrode during mechanical polishing. The particle and its surrounding aluminum also behave as a microcouple. The formation of a crevice is seen at the Al/Cu interface and copper redeposition occurred on the aluminum part not far from the copper particle. Furthermore, these results are in good agreement with those obtained on AA2024, in which Al_2CuMg particles act as copper sources after immersion in sulfate solutions with or without chlorides.[13]

Further SEM observations allow the zone close to the interface to be more accurately described. In Fig. 7a and b, the gray zone corresponds to aluminum while the white zone corresponds to copper. The deep crevice previously observed using optical microscopy was more accurately seen on the SEM micrographs. Moreover, aluminum was found to be corroded close to the Al/Cu interface, with a dissolution depth decreasing from the interface to some micrometers from the interface (Fig. 7a). Except in this zone, aluminum was not corroded. Similar observations were performed for copper, for which no corrosion damage on the copper disk except at the Al/Cu interface was seen (Fig. 7b). Accurate analysis of the topography of the copper at the interface gave striking results for the corrosion process. At the Al/Cu interface, copper formed a kind of ledge, with no corrosion damage on the copper disk surface but a strong dissolution of copper at the Al/Cu interface, suggesting the occurrence of crevice corrosion of copper.[33]

Comparison between theoretical calculations and experimental observations.— Observations of the morphology of the Al/Cu interface after immersion in the electrolyte suggest that corrosion occurs in different steps. The strong dissolution of aluminum at the Al/Cu

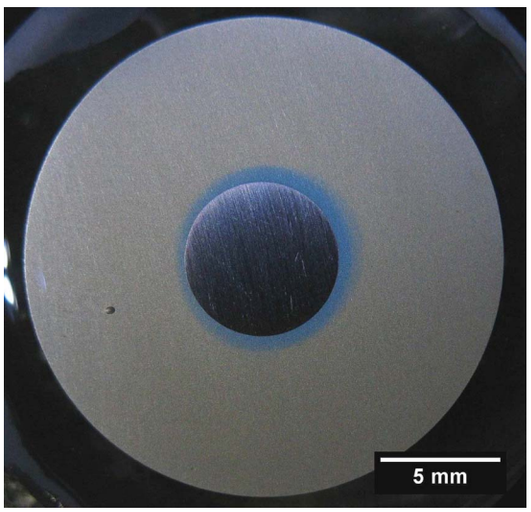

Figure 8. (Color online) Observation of the disk electrode during immersion in a 10^{-3} M Na_2SO_4 solution. Bromothymol blue was added to the electrolyte.

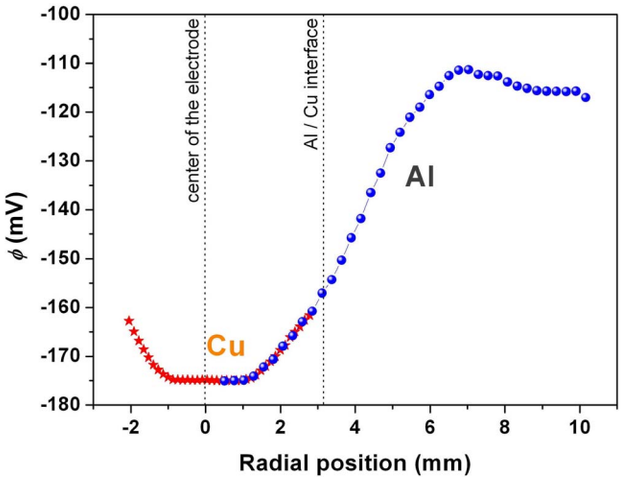

Figure 9. (Color online) Potential distributions measured in a 10^{-3} M Na_2SO_4 solution on the surface of the pure aluminum/pure copper model couple using a Ag/AgCl microreference electrode. Two consecutive measurements were performed.

interface partially leads to the formation of the crevice, as observed. Moreover, it can be assumed that, in the crevice, the chemical composition of the electrolyte varies significantly (occluded zone), leading to local chemical conditions which favor crevice corrosion of copper. The localized corrosion of copper explains the formation of the copper ring observed 150 μm from the interface. Thus, the initial step of the corrosion process appears to be the dissolution of aluminum at the Al/Cu interface, while aluminum remains passive on the remaining surface of the electrode. This is in good agreement with the current distribution previously shown from the numerical calculations (Fig. 4). A strong cathodic current density, related to increased reduction of the oxygen, was predicted on copper at the Al/Cu interface. Such a reaction should lead to a local alkalinization of the electrolyte.[32] To confirm this assumption, bromothymol blue was added to the 10^{-3} M Na_2SO_4 solution (pH 5.7) before immersion. This chemical turns blue when the pH exceeds a value of 7.6. Figure 8 shows a blue ring all around the disk electrode at the Al/Cu interface. The blue ring was formed only a few minutes after immersion of the disk electrode, indicating a fast and local increase of the pH of the electrolyte. This result shows that the kinetics of the cathodic reduction of oxygen was strong enough at the Al/Cu interface to induce a significant variation of the pH in the electrolyte.

Figure 9 shows the potential distribution measured in the 10^{-3} M Na_2SO_4 solution at the beginning of immersion at the surface of the disk electrode using a Ag/AgCl microreference electrode. The conductivity of the electrolyte was 10^{-6} S/m, but this value can be locally modified with time due to the corrosion reactions occurring on the disk electrode. Two consecutive measurements were performed and both gave the same results. The curves were also in good agreement with the potential distribution deduced from the theoretical calculations (z = 0.315 mm) (Fig. 3), showing that the hypothesis of the calculations was relevant. Thus, from these results, a three-step mechanism is proposed to explain the corrosion phenomena observed on the aluminum/copper model couple.

1. Step 1: During the immersion of the disk electrode in the electrolyte, aluminum is the anode of the system and is in the passive state, while copper is cathodically polarized. The current distribution shows that a significant oxygen reduction occurs on the copper electrode close to the Al/Cu interface, whereas copper dissolution can be ignored during the first moments of immersion. Thus, due to the strong cathodic reduction, alkalinization of the electrolyte occurs locally.

2. Step 2: When the pH reaches a value of 9, the aluminum depassivates and dissolves, leading to the formation of a crevice. The current distribution shows that the high cathodic current is restricted to the Al/Cu interface, which explains why the dissolution of aluminum only occurs at the Al/Cu interface, leading to the specific topography observed with SEM.

3. Step 3: In the bottom of the crevice formed by aluminum dissolution, local variation of the chemical composition of the electrolyte can occur because this is an occluded zone. Then, local chemical conditions enable crevice corrosion of the copper. Finally, dissolved copper can form a deposit on the disk electrode. The place on which copper forms the deposit depends on the potential distribution. Additional experiments were performed with copper sulfate; the aluminum/copper model couple was immersed in sulfate solution, copper sulfate was added, and a copper ring rapidly formed on the disk electrode, showing that when copper ions are present in the electrolyte, they can easily form deposits on the disk electrode at the right potential.

Such phenomena are not dependent on the scale of the events (Fig. 6), and the three-step mechanism could explain the corrosion mechanisms in commercial alloys such as AA2024 and why the dissolution of copper-rich intermetallics occurs independently of the nature of the electrolyte.[34] Indeed, the results showed that the most significant feature was the potential distribution, which provokes the increase of oxygen reduction at the interface and thus induces a strong variation of the pH of the electrolyte. Our study shows that a simple model (pure aluminum/pure copper) is relevant for the study of what happens in copper-rich aluminum alloys and also underlines the specific and important role of the Al/Cu interface. This feature cannot be observed if the galvanic coupling is studied in the usual way with two independent electrodes with electrical contact in the same solution.

Conclusion

The results show that studying such a simple system as the pure aluminum/pure copper couple is relevant to understand the corrosion phenomena associated with copper-rich intermetallics in aluminum alloys. The potential and current distributions on the surface of the model couple were deduced from theoretical calculations and the potential distribution was checked using a Ag/AgCl microreference electrode. Increased cathodic activity related to oxygen reduction was observed at the Al/Cu interface from the beginning of immersion. Combination of the measurements and calculations with optical and SEM observations of the model couple after a longer immersion time (24 h) allowed a three-step mechanism to be proposed

to explain the corrosion damage. In this mechanism, the formation of a copper deposit, always observed on commercial copper-rich aluminum alloys, does not appear to be the main step of the process but only a consequence of the corrosion damage. Our work underlines that the local alkalinization of the electrolyte at the Al/Cu interface plays a key role in the degradation of the system.

Acknowledgments

The authors gratefully acknowledge Yannick Thebault for his valuable assistance in SEM-EDS.

Centre National de la Recherche Scientifique assisted in meeting the publication costs of this article.

References

1. Z. Szklarska-Smialowska, *Corros. Sci.*, **41**, 1743 (1999).
2. J. W. J. Silva, A. G. Bustamante, E. N. Codaro, R. Z. Nakazato, and L. R. O. Hein, *Appl. Surf. Sci.*, **236**, 356 (2004).
3. A. Garner and D. Tromans, *Corrosion (Houston)*, **35**, 55 (1979).
4. X. Zhao, G. S. Frankel, B. Zoofan, and S. Rokhlin, *Corrosion (Houston)*, **59**, 1012 (2003).
5. M. Posada, L. E. Murr, C. S. Niou, D. Roberson, D. Little, R. Arrowood, and D. George, *Mater. Charact.*, **38**, 259 (1997).
6. M. R. Bayoumi, *Eng. Fract. Mech.*, **54**, 879 (1996).
7. X. Liu, G. S. Frankel, B. Zoofan, and S. Rokhlin, *Corros. Sci.*, **49**, 139 (2007).
8. I. L. Muller and J. R. Galvele, *Corros. Sci.*, **17**, 179 (1977).
9. J. F. Li, Z. Ziqiao, J. Na, and T. Chengyu, *Mater. Chem. Phys.*, **91**, 325 (2005).
10. J. Galvele and S. De Micheli, *Corros. Sci.*, **10**, 795 (1970).
11. V. Guillaumin and G. Mankowski, *Corros. Sci.*, **41**, 421 (1998).
12. W. Zhang and G. S. Frankel, *Electrochim. Acta*, **48**, 1193 (2003).
13. C. Blanc, B. Lavelle, and G. Mankowski, *Corros. Sci.*, **39**, 495 (1997).
14. C. Blanc, S. Gastaud, and G. Mankowski, *J. Electrochem. Soc.*, **150**, B396 (2003).
15. R. G. Buchheit, R. P. Grant, P. F. Hlava, B. McKenzie, and G. L. Zender, *J. Electrochem. Soc.*, **144**, 2621 (1997).
16. P. Campestrini, E. P. M. van Westing, H. W. van Rooijen, and J. H. W. de Wit, *Corros. Sci.*, **42**, 1853 (2000).
17. T. Dimogerontakis, L. Kompotiatis, and I. Kaplanoglou, *Corros. Sci.*, **40**, 1939 (1998).
18. P. Schmutz and G. S. Frankel, *J. Electrochem. Soc.*, **145**, 2295 (1998).
19. R. G. Buccheit, M. A. Martinez, and L. P. Montes, *J. Electrochem. Soc.*, **147**, 119 (2000).
20. R. G. Buchheit, L. P. Montes, M. A. Martinez, J. Michael, and P. F. Hlava, *J. Electrochem. Soc.*, **146**, 4424 (1999).
21. N. Birbilis and R. G. Buchheit, *J. Electrochem. Soc.*, **152**, B140 (2005).
22. C. Blanc, A. Freulon, M. C. Lafont, Y. Kihn, and G. Mankowski, *Corros. Sci.*, **48**, 3838 (2006).
23. Y. Yoon and R. G. Buchheit, *J. Electrochem. Soc.*, **153**, B151 (2006).
24. D. Zhu and W. J. van Ooij, *Corros. Sci.*, **45**, 2163 (2003).
25. T. Suter and R. C. Alkire, *J. Electrochem. Soc.*, **148**, B36 (2001).
26. M. Shao, Y. Fu, R. Hu, and C. Lin, *Mater. Sci. Eng., A*, **344**, 323 (2003).
27. R. S. Lillard, P. J. Moran, and H. S. Isaacs, *J. Electrochem. Soc.*, **139**, 1007 (1992).
28. J. Idrac, C. Blanc, Y. Kihn, M. C. Lafont, G. Mankowski, P. Skeldon, and G. Thompson, *J. Electrochem. Soc.*, **154**, C286 (2007).
29. Y. Liu, E. A. Sultan, E. V. Koroleva, P. Skeldon, G. E. Thompson, X. Zhou, K. Shimizu, and H. Habazaki, *Corros. Sci.*, **45**, 789 (2007).
30. S. Garcia-Vergara, P. Skeldon, G. E. Thompson, P. Bailey, T. C. Q. Noakes, H. Habazaki, and K. Shimizu, *Appl. Surf. Sci.*, **205**, 121 (2003).
31. N. Dimitrov, J. A. Mann, and K. Sieradzki, *J. Electrochem. Soc.*, **146**, 98 (1999).
32. N. B. Vukmirovic, N. Dimitrov, and K. Sieradzki, *J. Electrochem. Soc.*, **149**, B428 (2002).
33. K. Habib, *Opt. Lasers Eng.*, **31**, 13 (1999).
34. G. Boisier, C. Blanc, and N. Pébère, *Corros. Sci.*, Submitted.